PERGAMON

Journal of Structural Geology 25 (2003) 1507–1523

JOURNAL OF STRUCTURAL GEOLOGY

www.elsevier.com/locate/jsg

Mechanical behaviour of the Árnes and Hestfjall Faults of the June 2000 earthquakes in Southern Iceland: inferences from surface traces and tectonic model

Françoise Bergerat*, Jacques Angelier

Laboratoire de Tectonique, UMR 7072 CNRS-UPMC, case 129, 4, place Jussieu, 75252 Paris cedex 05, France

Received 11 October 2001; received in revised form 5 March 2002; accepted 9 October 2002

Abstract

Two major earthquakes ($M_S = 6.6$) occurred on June 17th and 21st, 2000 in southern Iceland. This paper presents mapping and measurements of representative segments along their surface fault traces: the Árnes Fault (June 17th) and the Hestfjall Fault (June 21st). The rupture trace of the Árnes Fault at Mykjunes shows a conjugate strike-slip pattern with a N30°E-trending right-lateral fault and a N60°E-trending left-lateral fault. Each of these faults is formed by en-échelon arrays of fractures and push-ups. The compression observed in the push-ups is inferred to represent the lateral displacement across the fault, which can be quantified by treating the push-ups as a shortening problem. Thus the mapped push-ups indicate an average strike-slip offset of 0.22 m for both these faults. The surface trace of the Hestfjall fault near Bitra reveals a N50°–60°E trending left-lateral strike-slip fault including large open fractures, N25°–35°E-trending en-échelon fractures and some push-ups indicating a left-lateral offset of 0.50–0.60 m along the Bitra fault segment. Two other fault segments on the Hestfjall Fault, near Eyvik and near Torfagil, show association of open fractures and normal faults. The most characteristic feature of the June 2000 fault traces is the en-échelon arrangement of fractures and push-ups. The 2000 rupture traces are compared with some historical seismic fault traces of the South Iceland Seismic Zone in terms of scale hierarchy of fracture traces. According to our observations at Bitra and Mykjunes, the general fault map of the *Orkustofnun* (National Energy Authority in Iceland) is interpreted as a conjugate system of strike-slip faults. A deformation model is proposed, aiming at reconciling the simple velocity boundary conditions imposed by plate kinematics along the left-lateral, E–W-trending transform zone, and the brittle deformation inside the South Iceland Seismic Zone. The observations made along the Árnes and Hestfjall Faults show that the actual earthquake-related fault pattern is not restricted to the N–S-trending dextral strike-slip revealed by focal mechanisms and N–S alignment of aftershocks, but includes conjugate systems consistent with the structural pattern of the South Iceland Seismic Zone.

Keywords: June 2000 earthquakes; Seismic faults; Surface traces; Iceland

1. Introduction

In southern Iceland, two major earthquakes ($M_s = 6.6$; Fig. 1) occurred on June 17th and 21st, 2000, ending nearly 100 years of relative seismic quiescence. Since the 11th century and prior to June 2000, a total of 33 major earthquakes, which caused the complete collapse of houses, had occurred in the South Iceland Seismic Zone (SISZ). The last sequences of major earthquakes took place on August 26th and 27th and September 5th and 6th, 1896, in the eastern and central parts of the zone, with magnitudes estimated between 6.9 and 6.0, and on May 6th, 1912 at its eastern tip ($M = 7$; Karnik, 1969). The June 17th and 21st, 2000 earthquakes were felt 200 km from their epicentres. Although no death, serious injury or complete house structural failure of buildings occurred, several houses were very badly cracked and subsequently abandoned. Some pipelines were broken. Hydrothermal activity increased around the faults and the Great Geyser (Geysir, Fig. 1), which had remained quiet for more than half a century, started to gush water and steam (Stefansson et al., 2000).

In this paper we present detailed maps and measurements of four representative segments of the surface traces of the

* Corresponding author. Tel.: +33-1-44-27-34-43; fax. +33-1-44-27-50-85.

E-mail address: francoise.bergerat@lgs.jussieu.fr (F. Bergerat).

0191-8141/03/$ - see front matter © 2003 Elsevier Science Ltd. All rights reserved.
PII: S0191-8141(02)00168-2

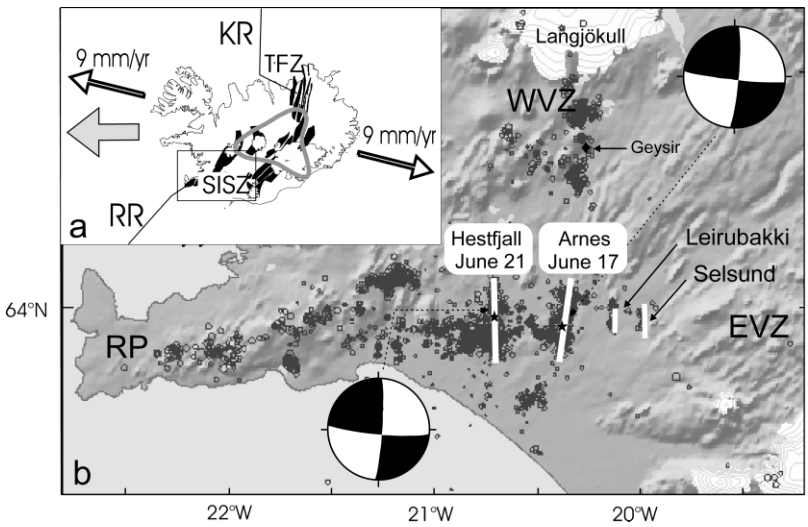

Fig. 1. The south Iceland Seismic Zone and the June 17th and 21st 2000 earthquakes. (a) Location of Iceland and the Mid-Atlantic Ridge. Icelandic rift zones in black, approximate contour of the Icelandic hot spot shown as grey line. SISZ: South Iceland Seismic Zone. TFZ: Tjörnes Fracture Zone. KR: Kolbeinsey Ridge. RR: Reykjanes Ridge. Open arrows indicate direction and velocity of plate divergence according to DeMets et al. (1990, 1994). Large grey arrow refers to the eastward motion of the Mid-Atlantic Ridge relative to the hot spot. (b) The two large earthquakes of June 17th and 21st 2000 (modified after Stefansson et al., 2000). Epicentres of these earthquakes as black stars, aftershocks as small open dots. Major earthquake fault zones as thick white lines for the June 2000 earthquakes (Árnes and Hestfjall faults) and two historical earthquakes of the eastern SISZ (Leirubakki and Selsund faults). RP: Reykjanes Peninsula. WVZ: Western Volcanic Zone. EVZ: Eastern Volcanic Zone. Focal mechanisms of the two major June 2000 earthquakes shown as stereoplots, with compression in the white quadrants.

two faults of the June 2000 earthquakes, called the Árnes Fault (June 17th) and the Hestfjall Fault (June 21st). We characterise the mechanical behaviour of these faults and integrate them in the geodynamical context of the SISZ. Detailed mapping of these fault traces was facilitated by a Trimble GPS Pathfinder Pro XRS differential system and completed by measurements of characteristic features with tape and compass.

The surface ruptures were observed and mapped about one month after the earthquakes. The surface traces of the earthquakes were still visible in the grassy soils of the affected area, whereas the disorders affecting the asphalt roads had been repaired in the few days after the earthquakes. Most fault traces were observed in the meadows and moors just before the open fissures were filled in and the scarps smoothed by the farmers.

2. Geodynamical context

Tectonic and magmatic activity in Iceland is controlled by two major geodynamical phenomena: the location above a major mantle thermal anomaly, the Iceland Mantle Plume, and the spreading of the Mid-Atlantic Ridge (Fig. 1a). Plate separation in Iceland occurs along a N105°E trend at a rate of 1.8 cm/year, according to the NUVEL-1 global plate motion model (DeMets et al., 1990, 1994). The general spreading axis of the Mid-Atlantic Ridge is moving westwards with respect to the Iceland Plume, so that new rift zones developed in the region above the plume when the plate boundary had migrated at a critical distance from it. Therefore, the axial rift zone in Iceland has repeatedly been shifted eastwards during the Late Cenozoic (e.g. Ward, 1971; Saemundsson, 1974; Helgason, 1985). These rift jumps have lead to the development of two major ocean-ridge discontinuities referred to as transform zones: the Tjörnes Fracture Zone (TFZ) in North Iceland, and the South Iceland Seismic Zone (SISZ) in South Iceland (Fig. 1a). Both these zones are characterised by high levels of seismotectonic activity.

The E–W-trending SISZ, centred at 64°N, is located at the junction of three rift-zone segments, forming a complex pattern (Fig. 1): to the southwest, the on-land extension of the Reykjanes Ridge in the Reykjanes Peninsula (RP), to the northwest, the Western Volcanic Zone (WVZ), and to the east, the Eastern Volcanic Zone (EVZ). Ward (1971) proposed that the SISZ is a left-lateral transform fault zone. There is, however, no major E–W-trending fault in South Iceland. Based on analysis of minor and micro-earthquakes, for periods of years or decades, the seismicity of the SISZ was essentially confined to a zone that is about 20 km wide from north to south and 70 km long from west to east (Stefansson et al., 1993; Bödvarsson et al., 1996). Consideration of the traces of major destructive earthquakes in the SISZ indicated that the N–S width is more likely to be several tens of kilometres (Gudmundsson, 1995). During the last few centuries, 33 sequences of large earthquakes ($M = 6–7$) occurred in the SISZ, at intervals of 45–112 years. These earthquakes have mostly been associated with N–S-trending right-lateral strike-slip faults arranged side-by-side (Einarsson et al., 1981; Einarsson and Eiriksson, 1982). However, a conjugate fault pattern was

demonstrated by Saemundsson (1978) in South Iceland and a number of ENE–WSW faults are shown on geological maps (Johannesson et al., 1990).

3. Methodology

Detailed maps of some fault segments associated with the June 17th and 21st earthquakes were made with a Trimble GPS Pathfinder Pro XRS differential system. The GPS receiver automatically calculates and stores, with sub-metric accuracy, the positions of different features such as points, lines and areas. This allowed us to accurately record the positions, shapes and elevations of all fault-related structures. We post-processed the carrier phase data in order to obtain an accuracy better than 10 cm (1–2 cm in the horizontal plane, and 2–5 cm in the vertical direction). Because of the irregularities in the soil surface, it was sometimes difficult to measure directly with the GPS system some characteristic features, therefore we made additional measurements using compass, clinometer and a measuring tape. Most of these measurements included (1) the vertical offsets along each fracture, (2) the width of particular structures such as open fissures, and (3) the height and shape of the push-ups.

Because the soil layer may have collapsed in the open fractures, or slipped because of the slope, the apparent opening of the fractures can be smaller or larger than the actual opening (Fig. 2a). Therefore, the width of open fractures was in most cases measured (1) beneath the soil layer, where the upper basaltic lava flow was observable, in order to determine the actual dilation of the fissure, and (2) where it reached a maximum value, generally halfway along each open fracture.

Small push-ups commonly developed along the June 2000 earthquake faults (Fig. 2b). Cross-sections of these push-ups were observed in many cases along the open tension-shear fractures that trend perpendicular, or oblique at large angles, to the push-up axis. These cross-sections revealed that the push-ups simply affect the soil layers, which accommodate the compressional deformation by concentric folding, not internal compression of soil. This mechanical behaviour of the soil layers gave easy access to determinations of shortening across the push-ups. Measuring the shortening across the push-up structures was important because it allowed us to evaluate the horizontal offset of strike-slip faults, which is difficult to determine otherwise. Where the push-ups were well individualised, both the length of their surface envelope (E_0) and the width of the same push-up (E) were measured along appropriately oriented cross-sections (Fig. 2c). The amount of shortening, ΔE, calculated in the direction perpendicular to the push-up axis, and hence the slip of the fault, was given by:

$$\Delta E = E_0 - E \quad (1)$$

4. The June 17th and 21st, 2000 earthquakes and their surface traces

Detailed information about the location and magnitudes of these earthquakes, the ground acceleration data, the hydrothermal activity, etc., can be found on the Internet sites of the Department of Geophysics of the Icelandic Meteorological Office (IMO) (http://hraun.vedur.is/ja/englishweb/index.html), the Earthquake Engineering Research Center of the University of Iceland (http://www.afl.hi.is), the National Earthquake Information Center (NEIC) of the USGS (http://www.neic.cr.usgs.gov/neis/bulletin/bulletin.html), and the National Energy Authority in Iceland (http://www.os.is).

The National Energy Authority (*Orkustofnun*) presented a map with the location and trends of about 40 'fissure segments' (i.e. surface traces) that were quite visible in the few days following the June 2000 earthquakes (Fig. 3). The trends of these traces range between N0°E and N65°E. At a regional scale, the traces are arranged en-échelon along two about N–S-trending lines, 25 km long, called the Árnes Fault and the Hestfjall Fault (Fig. 3). This en-échelon pattern seems consistent with right-lateral motion along the two main faults. In addition, a left-lateral en-échelon pattern of fissures near Bitra may be interpreted as indicating left-lateral shear along a nearly E–W trend, although the angle between the fissures and this trend is large. This inference was important from the structural point of view, because such a left-lateral fault zone would form a conjugate pattern with the right-lateral Hestfjall Fault (Fig. 3), and thus needed confirmation. At some locations the map shows two 'fissure segments' that cross at an acute angle of about 40°, a pattern resembling a system of conjugate strike-slip faults. As a consequence, one of our field targets consisted of determining the orientations and senses of slip along some of these diversely oriented fissures, to check the hypothesis of conjugate fault pattern occurrence at different scales.

We present herein the description and analysis of surface traces at four main localities shown in Fig. 3. The first locality is Mykjunes along the Árnes Fault; the other three localities are near Eyvik, near Bitra and in the Hestfjall mountain, all located along the Hestfjall Fault.

4.1. The Árnes Fault

The June 17th, 2000 earthquake occurred at 15:40 GMT, centered on a focus located at 63.97°N–20.36°W, with a depth of 6.3 km (Stefansson et al., 2000). The earthquake fault is named the Árnes Fault. From modelling using volumetric strainmeters, the IMO proposed a moment

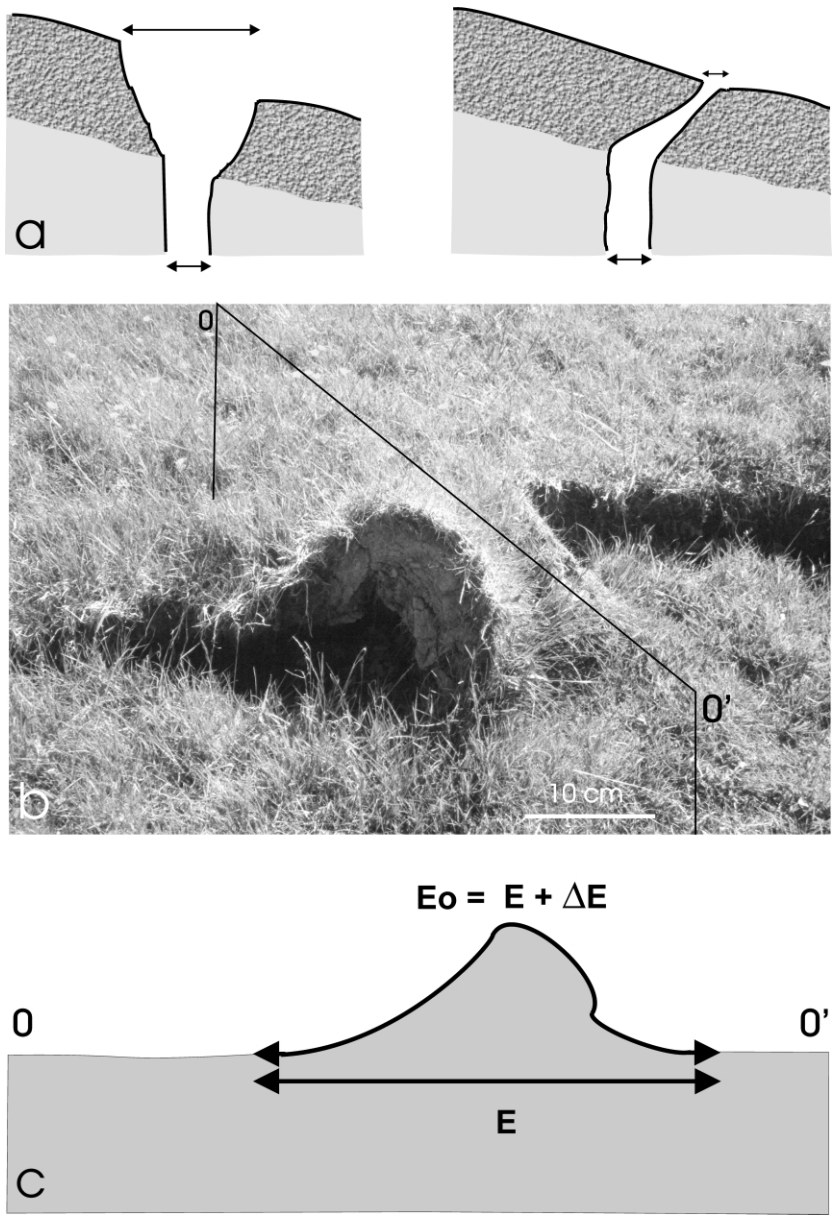

Fig. 2. Some representative surface features of the June 2000 earthquake fault traces. (a) Schematic cross-sections of earthquake fissures. Note that the apparent width of the fissure in the soil layer (rugged grey pattern) may not reflect the actual fissure width (and hence the dilation) in the bedrock (light grey). It can be larger (on left) or smaller (on right). See text for discussion. Variable scale: the fissure width in the bedrock varies from 0.02 to 1 m in the measurement sites. (b) Photograph of a small push-up structure in the grassy soil along the right-lateral fault segment at Mykjunes. View perpendicular to fault trace. Note the folded soil layer (centre of photograph). (c) Schematic cross-section of a push-up, located as O–O′ in (b). The final width measured is E, the corresponding width before push-up formation is given by measuring the surface envelope of the push-up, E_0. The shortening across the push-up, $\Delta E = E_0 - E$, indicates the offset of the strike-slip fault.

magnitude $M_w = 6.4$, noting however that the single fault model used did not comply with all the data and indicated a more complicated model than a single strike-slip fault (Stefansson et al., 2000). The preliminary surface wave magnitude given by the NEIC was $M_s = 6.6$. According to the IMO seismic database, aftershocks of this earthquake indicate a 16 km long fault plane, striking approximately N9°E and dipping 86° towards the east, down to 10 km depth. According to the map of the National Energy Authority, surface fissures are found in a 25 km N–S elongated area (Fig. 3), coinciding with the aftershock area and indicating a right-lateral motion.

The surface traces presented herein as an example are located at 63°56′22′N and 20°21′09′W, near the Mykjunes Farm. The surface mapping of the June 17th, 2000 earthquake traces in this locality (Bergerat and Angelier, 2001) revealed the presence of a conjugate strike-slip pattern, including a N30°E-trending right-lateral fault segment and a N60°E-trending left-lateral one (Fig. 4). The minor features indicating the strike-slip senses in the

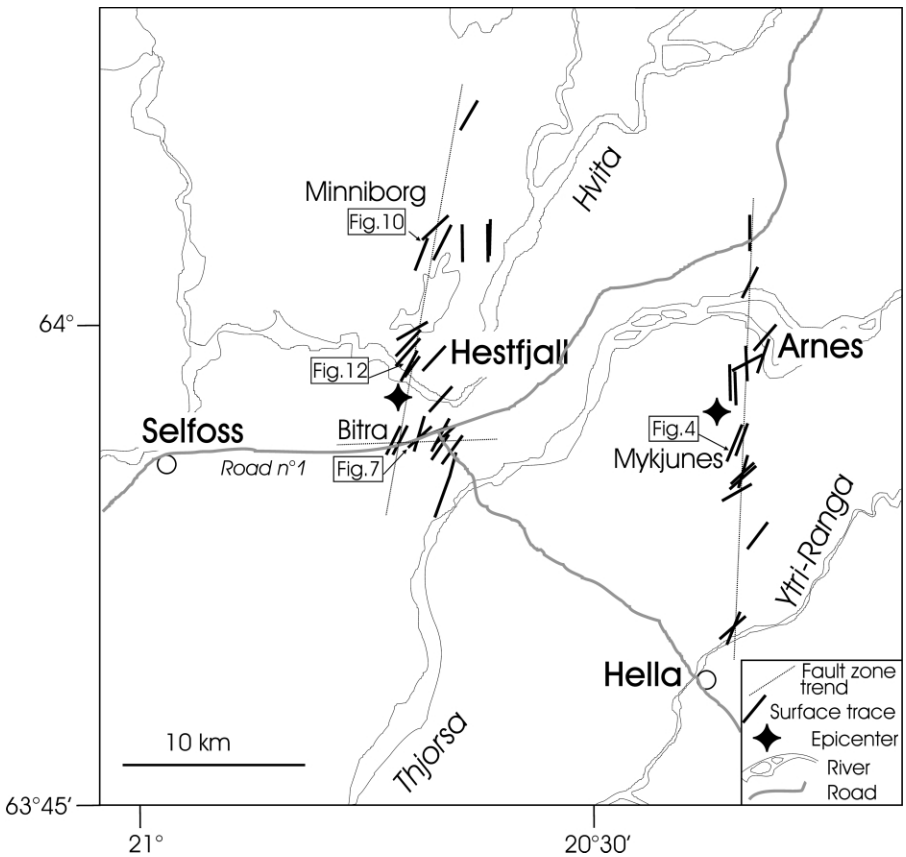

Fig. 3. Map of the surface fissures (thick black lines) of the June 17th and 21st 2000 earthquakes, modified after the map of the National Energy Authority (*Orkustofnun*, Reykjavik, Iceland: http://www.os.is/english/). The axes of the main fault zones, right-lateral (Árnes Fault of June 17th and Hestfjall Fault of June 21st) and left-lateral (Bitra Fault of June 21st) are added as thin lines according to the discussion in this paper. Location of Figs. 4, 7, 10 and 12 are indicated (maps of Mykjunes, Bitra, Eyvik and Torfagil surface traces, respectively).

mapped area are illustrated in Fig. 5. The senses of strike-slip motion were unambiguously determined for both these fault segments, based on the en-échelon arrangements of fissures and push-ups (Fig. 5d and e). The faults traces have been continuously mapped along distances of about 200 m. Out of the mapped area, no trace was recognised south-west of the junction of segments; to the north-east the traces are discontinuous because the surface of the meadows becomes irregular, with a dense pattern of hummocks (*thufurs*) and an undulating topography.

Each of the structural fault segments is constituted by en-échelon arrays of fractures, which are themselves formed by en-échelon individual fractures and push-ups (Figs. 4 and 5b and c). Within the mapped area, five arrays of fractures have been identified along the right-lateral fault segment and three along the left-lateral one. The length of the arrays of fractures ranges between 16 and 59 m (35 m on average) and most individual fractures are 1–3 m long. The average azimuth of the arrays of fractures is N40°E on the right-lateral fault segment where the individual fractures trend N45°–50°E. On the left-lateral fault segment, the arrays of fractures trend N45°E on average while the individual fractures strike N25°–30°E. Note that the N45°E direction may correspond to dextral or sinistral motions according to the segment considered, which tightly constrains the direction of compression. This is consistent with the tensile direction given by the fracture opening orientations, which range 120°–140°.

Most fault traces at Mykjunes reveal pure strike-slip. However, the northern part of the right-lateral fault segment shows a normal component associated with the dominating strike-slip motion (Figs. 4 and 5f and g). At this place, two fracture traces bound a 12–15-m-wide graben (Gr in Fig. 4), with vertical throws of 0.10–0.40 m on the western edge and 0.15–0.20 m on the eastern one. Whereas most of the dextral strike-slip motion is accommodated on the eastern fracture (AF5 in Fig. 4), as shown by en-échelon fissures, vertical displacement prevails on the western side.

The Mykjunes strike-slip fault traces show systematic occurrence of small push-ups as relay zones between the individual, en-échelon arranged, fractures (Fig. 4). The height of these push-ups ranges between 0.08 and 0.35 m (0.18 m on average) along the left-lateral fault segment. It ranges between 0.10 and 0.35 m (0.26 m on average) on the right-lateral one (Fig. 6a). Among a total of 61 mapped push-ups, 17 were chosen owing to their good state of preservation and accurately measured along both the left-lateral and the right-lateral fault

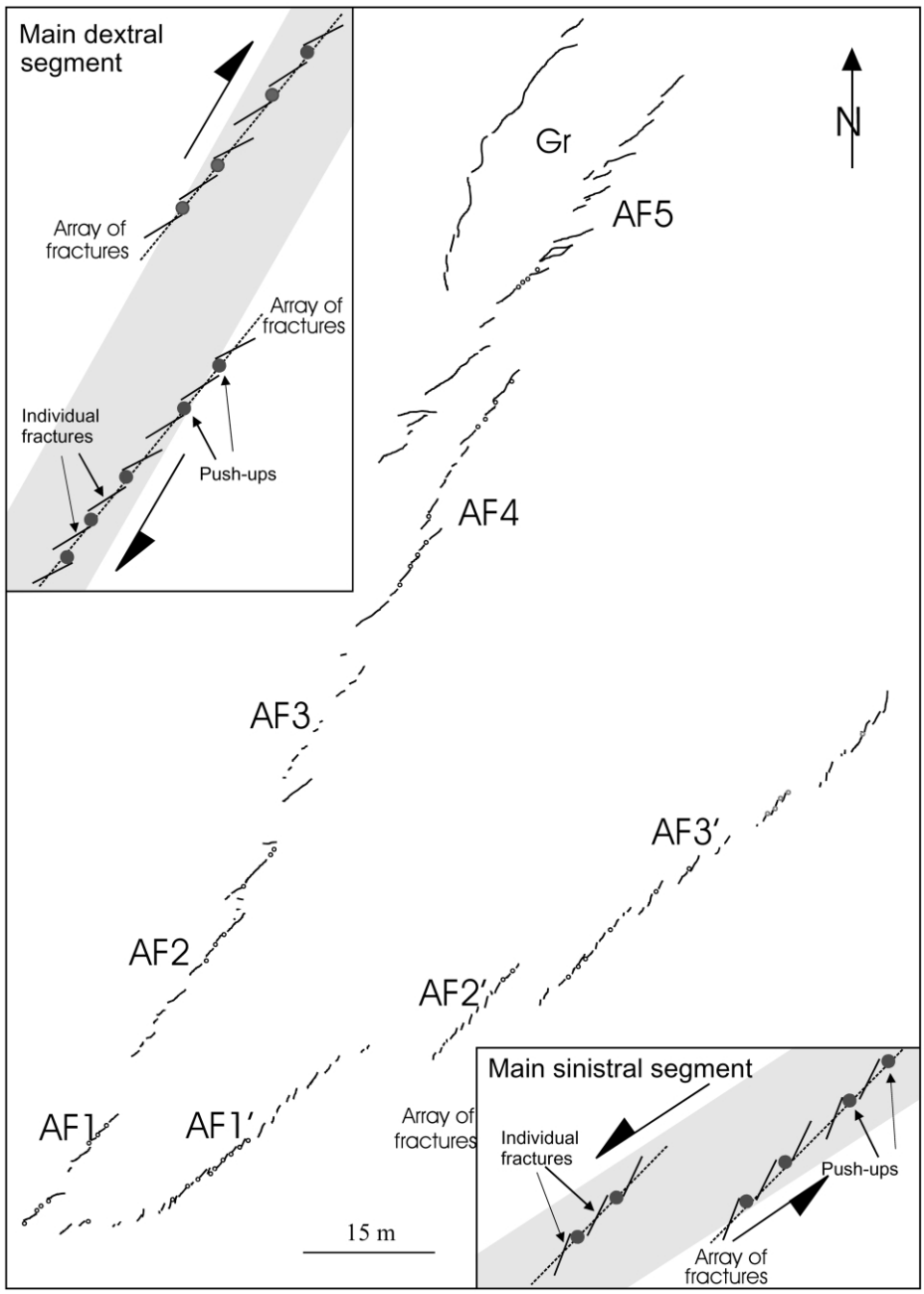

Fig. 4. Map of surface fissures of the June 17th, 2000 earthquake near Mykjunes (location in Fig. 3). Mapping done using kinematic GPS (see text). Open fractures as black lines, push-ups as open dots. Note the multiscale en-échelon patterns, with individual fractures forming several arrays along each fault segment. AF1–AF5: arrays of fractures along the right-lateral fault segment; AF1′–AF3′: arrays of fractures along the left-lateral fault segment; Gr: graben at the northern part of the right-lateral fault segment. Insets are schematic sketches of en-échelon patterns of fractures and push-ups for both the right- and left-lateral fault segments, with two arrays shown in each case. Deformation zone in grey.

segments, in order to estimate the horizontal shortening (Fig. 2c), and hence the amount of strike-slip motion. The amounts of shortening ranged between 0.10 and 0.27 m along the left-lateral fault, and between 0.18 and 0.39 m along the right-lateral one (Fig. 6b). In terms of average values and standard deviations, one concludes that the amounts of co-seismic strike-slip displacements were 0.17 ± 0.06 m for the left-lateral fault, and 0.25 ± 0.07 m for the right-lateral fault. In addition, the latter value is supported by one measurement in a small pull-apart structure, indicating a dextral strike-slip displacement of 0.22 m.

Our mapping of the June 17th earthquake fault traces at Mykjunes thus reveals the occurrence of a conjugate system of strike-slip fault movements, right-lateral along the N30°E direction and left-lateral along the N60°E one (Fig. 4), with almost equivalent amounts of relative displacement (0.25 and 0.17 m, respectively).

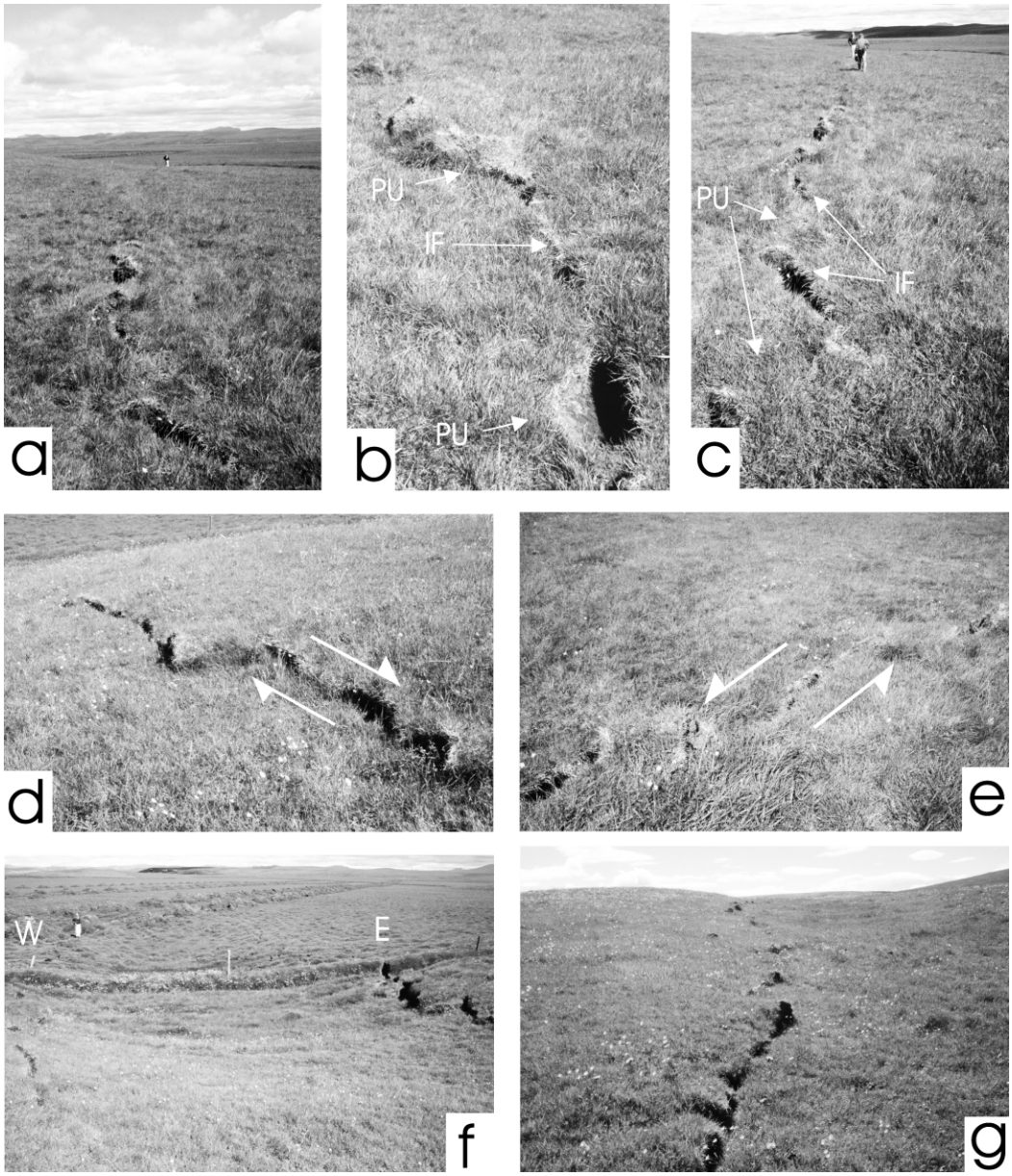

Fig. 5. Photographs of the surface traces of the 17th June 2000 earthquake near Mykjunes (see also Fig. 4). Views towards the NE or ENE, except the last photograph taken in the opposite direction. (a) View of the main left-lateral fault segment. (b) and (c) En-échelon distribution of individual fissures (IF) and push-ups (PU) along the right-lateral (b) and left-lateral (c) fault segments. (d) and (e) Relationships between push-ups and individual fissures, indicating right-lateral (d) and left-lateral (e) strike-slip movements. (f) Graben at the northern tip of the right-lateral principal fault segment (Gr in Fig. 4), with W and E indicating the western and eastern fissures and scarplets bounding the graben. (g) Western graben-bounding fracture, located at W in (g); the vertical throw reaches 0.25 m.

4.2. The Hestfjall Fault

The June 21st, 2000 earthquake occurred at 00:51 GMT, centered on a focus located at 63.97°N–20.71°W, with a depth of 5.1 km (Stefansson et al., 2000). The earthquake fault is named the Hestfjall Fault. The preliminary surface wave magnitude given by the NEIC was $M_s = 6.6$. Like the first earthquake, a more complicated source model than that routinely used in such calculations was indicated by strainmeter data modelling (Stefansson et al., 2000). According to the IMO database, the aftershocks of the June 21st earthquake indicate a 18 km long, nearly vertical fault that strikes N2°W, down to 8 km depth. According to the map of the National Energy Authority, the surface fissures developed along a N10°E-trending line, about 25 km long (Fig. 3), and indicate right-lateral motion. This line generally coincides with the aftershock area. As mentioned earlier, however, the distribution of the southernmost surface traces of the June 21st earthquake does not match the N10°E alignment, which suggests that the fracture pattern may be more complex than a single fault (Fig. 3). Along the Hestfjall Fault, three segments have been mapped

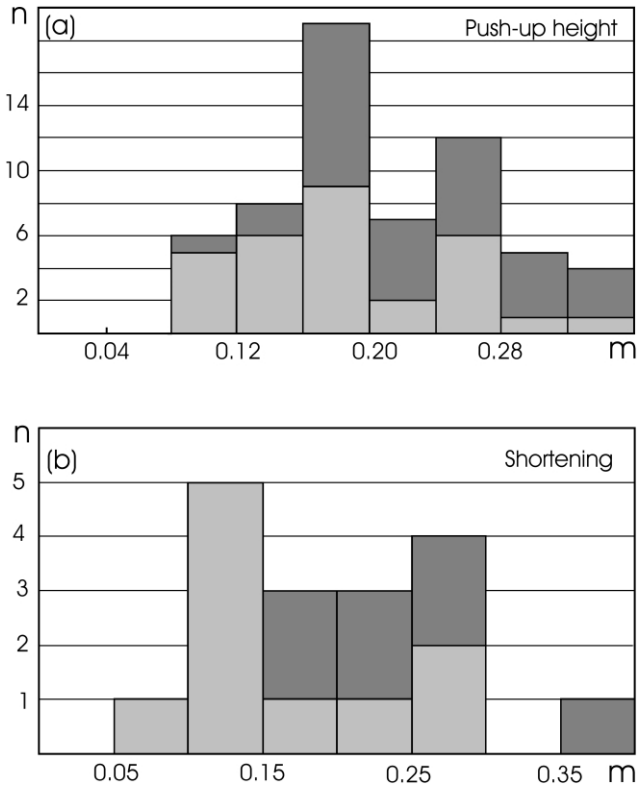

Fig. 6. Characteristics of the push-ups at Mykjunes (location in Fig. 3). (a) Number of data versus push-up height; (b), number of data versus shortening across push-ups. Data from the left-lateral segment in light grey, data from the right-lateral segment in dark grey.

in detail near the Bitra Farm, near Eyvik and in the Hestfjall mountain. They illustrate contrasting aspects of the surface traces of the June 21st earthquake.

4.2.1. The Bitra portion of the Hestfjall Fault

The surface traces of the Bitra fault segment are located at 63°57′06′N–20°42′29′W, close to the road no. 1 and near a small summerhouse (Bergerat and Angelier, 2001). These surface traces correspond to a N50°–60°E-trending left-lateral strike-slip fault, which has been mapped continuously over a distance of 250 m (Fig. 7). The earthquake fault trace could be followed at larger distances to the east and to the west, but, contrary to the area shown, the rugged topography did not allow high quality mapping. The mapped portion of the fault segment includes large open fractures, en-échelon fractures and push-ups (Fig. 8). West of the summer house (between the house and a small shed), the fault strikes N50°E on average. It is mainly composed of large open fractures that strike N40°–60°E (Fig. 8b) and some en-échelon N25°–35°E fractures (Fig. 8a). The width of these fractures ranges between 0.21 and 0.70 m (0.40 m on average). East of the summer house, the fault strikes N60°E on average. It is mainly composed of aligned push-ups (Fig. 8c) that often merge as small hillocks (Fig. 7a), and individual fractures that strike N5°E to N60°E and often display typical left-lateral en-échelon patterns (Figs. 7b and 8d). Farther to the east, typical fracture patterns can be identified although the ground surface is more irregular with *thufurs*. Some fractures strike N50°–60°E, parallel to the general trend of the fault trace, whereas open fractures that strike N20°–40°E form a left-lateral en-échelon pattern (Figs. 7c and 8e).

A total of 120 fractures were measured along the fault trace; 107 of these fractures were located east of the summer house, 97 of them being typical open fractures with widths in the range 0.02–1 m (0.23 m on average); the most common widths fall in the range 0.10–0.30 m (63% of open fractures, see Fig. 9). As mentioned above, the long open fractures west of the summer house display large widths (0.40 m on average). Because of ground collapse along fissure edges, the apparent width of these fractures at the surface is larger (Fig. 8b). In the whole mapped area, west and east of the summer house, most fractures show no or little vertical displacement. Amongst the 120 measured fractures, only four show significant vertical throw (0.30–0.40 m). In terms of fracture length, the longest fractures (about 5–15 m long) strike ENE–WSW, parallel to the general trend of the surface trace. The NNE–SSW-trending fractures have significantly smaller lengths (in the range 1–5 m), and they are arranged en-échelon, consistent with the left-lateral sense of motion along the surface trace (Figs. 7 and 8d).

Particular attention was paid to the push-up structures, because of their potential to reveal the amount of strike-slip displacement through shortening determinations (contrary to estimates based on open fissure dilation, which reveal high levels of dispersion). The heights of the 24 mapped push-ups range between 0.09 and 0.76 m (0.35 m on average). However, the coalescence of several push-ups (Fig. 7a) and in some cases the irregular topography (especially where *thufurs* were present) result in inaccurate measurements. For these reasons, only three well delineated push-ups in a flat meadow surface could be reliably measured with sufficient accuracy in terms of shortening estimates. A fourth datum, different in type, also allowed evaluation of the left-lateral displacement along the fault segment: the horizontal shift of the concrete foundation of the summer house, relative to its imprint in the ground. These four best defined measurements result in a strike-slip displacement ranging between 0.29 and 0.61 m, all in the left-lateral sense, with an average value of 0.47 m.

4.2.2. The Hestfjall Fault near Eyvik

We also analysed the surface traces of the Hestfjall Fault in a grassy and wooded gentle slope near a small summerhouse east of Eyvik. This site is located at 64°02′59′N–20°41′08′W near road no. 354, east of Minniborg (Fig. 3). This Eyvik fault segment has been mapped over a distance of about 100 m. Its trend is N140°E in the northern part of the mapped area, and N170°E in the southern part (Fig. 10a). The most important earthquake-related feature is a normal fault scarp (Fig. 11a). In the soil, the vertical throw varies

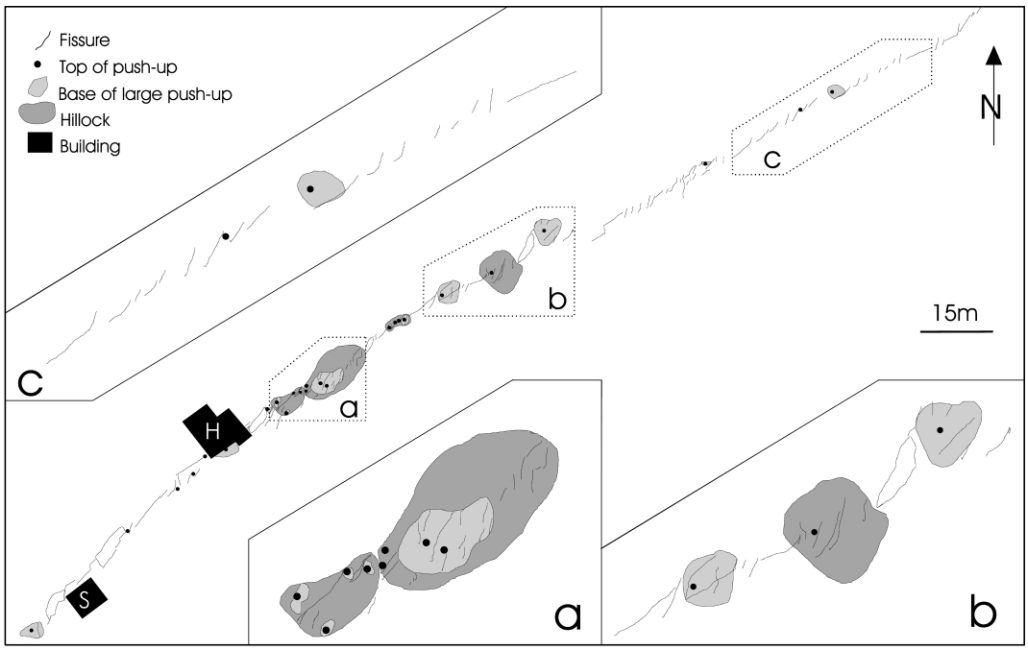

Fig. 7. Map of surface fissures of the June 21st 2000 earthquake near Bitra (location in Fig. 3). Mapping done using kinematic GPS (see text). H: summerhouse; S: shed. Open fractures as black lines, push-ups as light grey areas with top indicated by dot (smallest push-ups as dots alone). Where push-ups coalesce, the resulting hillocks are shown as dark grey areas. The three rectangles of the main map refer to the detailed maps (a)–(c).

from 0.4 to 1.4 m (1 m on average) in its central part. At least part of the vertical displacement reflects the surface sliding in the slope so that as far as deep fault tectonics effects are concerned the vertical throws of the fractures are certainly overestimated. Although the normal fault surface dips to the west, at some places the apparent fracture dip direction changes from west to east in the uppermost section, where the normal shear fault changes into an open fissure (Fig. 10, scarp sections 4–6). As a result, the surface scarp may resemble that of a reverse fault; however, the fracture opening data collected in the bedrock clearly indicate dilation consistent with a deeper normal shear. Such a near-surface transition from normal fault to open ground fracture has been described, at a wider scale, elsewhere in Iceland (Angelier et al., 1997).

Several open fractures developed in the footwall near to, and parallel with the normal fault scarp. Some of them show vertical offsets, indicating a combination of tensile opening and normal shear. Typically, most of these open fractures are located along the southern and northern portions of the main fault, which in map view exhibits a concave shape towards the footwall. The width of the open fractures at Eyvik ranges from 0.04 to 0.90 m (0.30 m on average). Their vertical throw, where present, varies from 0.10 to 0.43 m.

Along the Eyvik scarp, the fault surface itself could be observed in the soil. It dips 50°–70° to the west. Slickenside lineations were also found at some places (Figs. 10c and 11b). Note that all measurements indicate a consistent slip orientation (about N80°E, hanging wall relative to footwall) regardless of the variations in fault strike. The attitude of these striae indicate normal dip-slip motion of the fault where it strikes N–S, and oblique-slip with a minor right-lateral component where it strikes NW–SE according to the general geometry of the fault trace (Fig. 10b). The homogeneous attitude of the slip vectors on variously oriented surfaces of the same fault indicates E–W extension (note that the slip vector is the common axis for all measured fault planes).

4.2.3. The Hestfjall Fault at Torfagil

The third place where we analysed surface traces of the Hestfjall Fault was located along the Torfagil fault segment at 63°58′42′N–20°42′40′W, near the Hvita river, east of Skjolholar. At this site, the surface traces are visible in the southern side of the Hestfjall mountain, where the slope strikes N120°E and dips approximately 25°SW. The surface traces have been mapped over a length of about 50 m (Fig. 12). The fault segment trends N150°E on average, but is sinuous in detail. Most individual fractures strike N120°–140°E and N150°–180°E (38 and 41% of the total population, respectively). The fractures display associated opening and vertical offset (Fig. 11c); among a total of 38 measured open fractures, only seven have no vertical offset. The fracture width ranges from 0.03 to 0.45 m and the vertical offset ranges from 0.03 to 0.28 m (Fig. 12b). These fractures are arranged more or less en-échelon. Although no definite indication of strike-slip displacement emerges from their pattern (Fig. 12a), the distribution of fracture steps rather suggests that some right-lateral component of motion took place along the fault segment.

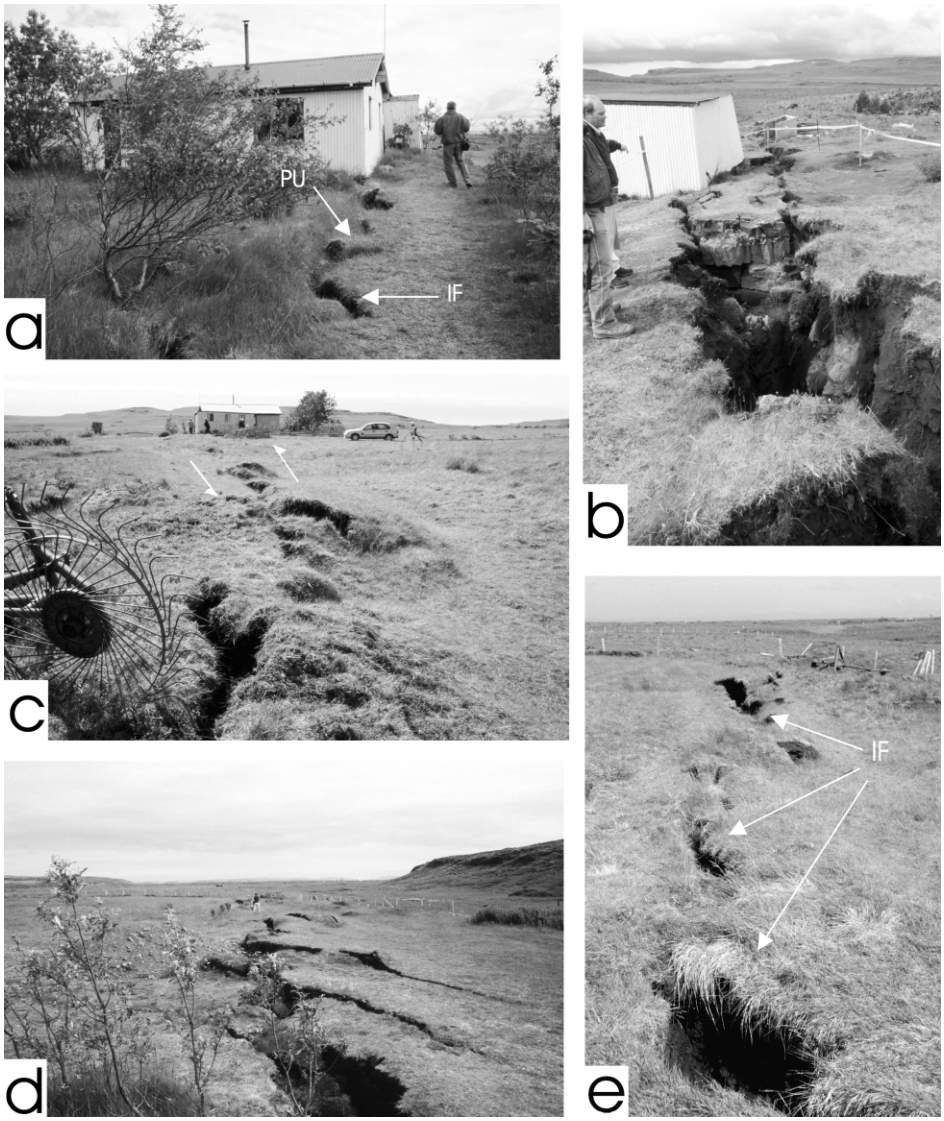

Fig. 8. Photographs of the surface traces of the 21st June, 2000 earthquake near Bitra (see also Fig. 7). Views towards the E (a, d and e) or the W (b and c). (a) Fault trace immediately west of the summerhouse, with en-échelon fractures (IF) and push-ups (PU) indicating left-lateral motion; (b) large open fracture between the summerhouse and the shed (visible in background), with surface width larger than actual bedrock dilation; (c) left-lateral fracture zone with en-échelon fissures and push-ups east of the summerhouse (in background); (d) en-échelon open fractures indicating left-lateral motion east of the summerhouse, with apparent vertical throw resulting from push-up development forming hillocks; (e) en-échelon pattern of open fissures (IF) along the left-lateral fracture near the eastern tip of mapped area.

5. Discussion

The only major earthquake of the 20th century in south Iceland was the 1912 earthquake at Selsund (M = 7), near the eastern tip of the SISZ. The surface traces of this 1912 earthquake, as well as those of older earthquakes, have been analysed a long time after their occurrence. The June 17th and 21st 2000 earthquakes thus provided the first opportunity to characterise freshly formed traces of major earthquakes in this region and to compare them with the traces of historical earthquakes. We then analyse the deformation patterns related to these last major earthquakes and we discuss the related distribution of the deformation within the frame of the rift–rift transform zone.

5.1. Characteristic strike-slip features and scale hierarchy of fracture traces

The analyses of the two fault segments at Mykjunes and Bitra show that for both the June 17th and 21st 2000 earthquakes, the surface traces are not simply related to right-lateral strike-slip faulting along N–S faults, as the seismological data would have suggested. These analyses demonstrate the existence of right-lateral faulting along NNE–SSW trends (Mykjunes) and left-lateral faulting along ENE–WSW ones (Mykjunes and Bitra). Although they are more difficult to interpret, complementary analyses at the other two localities, Eyvik and Torfagil, suggest that

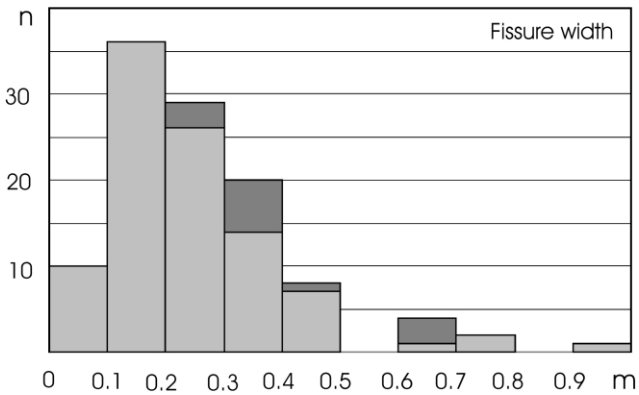

Fig. 9. Distribution of actual fissure width at Bitra (location in Fig. 3). Number of data versus fissure width. Note the difference in width distribution between the fault trace west (dark grey) and east (light grey) of the summerhouse.

extensional deformation producing open fractures and normal faults plays a role along the Hestfjall Fault.

The most characteristic features of the typical strike-slip fault segments are en-échelon open fractures and push-ups, as illustrated in Mykjunes and Bitra. In our study, these features were mainly observed in soils, but they are observable in the bedrock (aa or pahoehoe lavas) for some of the still visible surface traces of various historical earthquakes (Einarsson et al., 1981; Einarsson and Eiriksson, 1982), including the Selsund Fault (1912 earthquake; Bjarnasson et al., 1993) and the Leirubakki Fault (earthquake of unknown age; Bergerat et al., 2002). Although the aspect of the open fractures and push-ups depends on the nature of the surface layers, the same types of characteristic features were observed in most cases.

The N–S-trending historical seismic faults show an en-échelon arrangement of fractures and push-ups at various scales similar to that of the Árnes and Hestfjall Faults, and also characteristic right-lateral strike-slip motion. For example, the exposed surface rupture of the Leirubakki Fault (Bergerat et al., 2003) contains fractures that range in length over four orders of magnitude from the main fault, which is probably several tens of kilometres long, through fault segments (1000–2000 m long), fracture arrays (100–250 m long) to individual fractures (8–125 m long). Both the preliminary mapping of *Orkustofnun* for the first, largest, order of magnitude (Fig. 3) and our site mapping for the third and fourth orders of magnitude (Figs. 4 and 6) suggest that a similar scale distribution prevailed during the June 17th and 21st earthquakes, along the Árnes and Hestfjall Faults. However, between the scales of the main fault and the fracture array, an intermediate scale exists at Leirubakki: that of the fault segment, with an approximate length of 1000–2000 m. This intermediate scale was poorly distinguished in the case of the Árnes and Hestfjall faults because the outcrop conditions did not allow mapping of complete fault segments.

According to our observations, the fracture arrays at Mykjunes (20–60 m for the dextral arrays) are relatively small as compared with those of Leirubakki (100–250 m), and the individual fractures have lengths of 1–3 m at Mykjunes and about 10–100 m at Leirubakki. This observation raises the problem of the relation between the multiscale fracture pattern and the size of the earthquake that gave rise to the fracture traces. A possible interpretation implies that the lengths of the individual fractures and fracture arrays increase with the amount of slip, and hence with the earthquake magnitude. This interpretation would be in qualitative agreement with the contrast between the measured magnitudes of the June 2000 earthquake along the Árnes Fault ($M_w = 6.4$ according to Stefansson et al. (2000)) and the inferred magnitude of the historical Leirubakki earthquake (at least 7.1 according to Bergerat et al. (2003)). Another alternative implies that the 1–3-m-long open fissures affecting the soft soil layer at Mykjunes have no equivalent at Leirubakki, where the bedrock crops out at the surface. In this case, and assuming that at these scales there is no definite length-magnitude dependency, the 20–60-m-long fracture arrays that we describe at Mykjunes may partly correspond to the 8–125-m-long individual fractures described at Leirubakki. This would indicate the existence of a still smaller end-member in the scale hierarchy, at least where thin surface layers are present, suggesting that the thickness and mechanical properties of the near-surface layer also control the length distribution of the fractures. Such multiscale en-échelon arrangement of faults has been interpreted in terms of a depth hierarchy of deformation (Belardinelli et al., 2000; Bergerat et al., 2003) including the main fault at depth, subordinate buried faults near the surface and individual fractures in the uppermost layer (lava flow and/or soil).

5.2. Deep-seated faulting versus gravitational sliding

Because the surface traces of the Torfagil and Eyvik fault segments were observed in a mountain slope, the problem of their origin, deep-seated or shallow, deserves discussion. Gravitational sliding has certainly been triggered by the earthquake vibration and some surface slips of this kind have been observed near these two sites (K. Saemundsson, pers. comm.). For this reason, a large part of the vertical displacement probably reflects the surface sliding in the mountain slope, so that as far as deep fault tectonics effects are concerned the vertical throws of these fractures are certainly overestimated.

Based on our field analysis, we think that the dextral slip component on these two fault traces reflects the general behaviour of the Hestfjall Fault at depth, whereas, at the local scale, the extension responsible for normal faulting and fissure opening was greatly accentuated by gravity sliding.

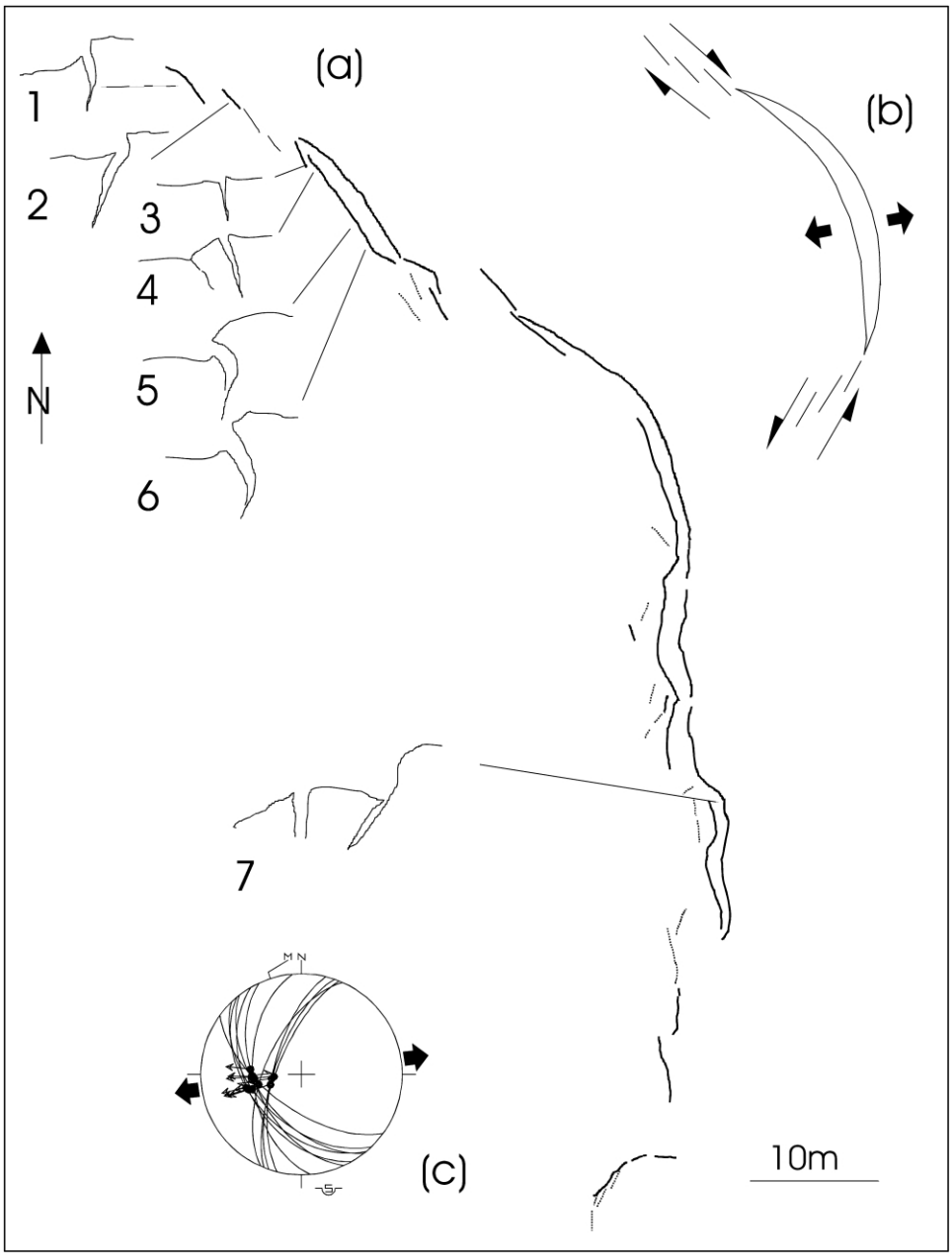

Fig. 10. Map of surface fissures of the June 21st 2000 earthquake at Eyvik (location in Fig. 3). Mapping done using kinematic GPS (see text). (a) Map of individual fissures as dotted lines and normal fault as solid line with both the upper and lower edges mapped along the largest scarp. Seven typical cross-sections of the scarp are added (note in sections 4–6 the apparent near-surface reversal of the fracture dip, revealing transition from the deep normal fault to the open ground fracture; (b) schematic representation of the geometry of the surface traces, which reflects downward-slipping of soil triggered by deep-seated tectonics; (c) stereoplot (Schmidt's projection, lower hemisphere) showing the fault slip data collected along the normal fault surface, including the fault planes as thin lines (note the azimuthal dispersion) and the slickenside lineations as small arrows (all normal, note the homogeneity in trend and dip). Large black arrows indicate the direction of extension.

5.3. Distribution of the deformation related to the June 17th and 21st 2000 earthquakes

We aim at characterising not only the mechanics of the Árnes and Hestfjall Faults, but also their role in the regional deformation. For that reason, it is interesting to quantify the deformation that occurred in the SISZ related to the June 17th and 21st 2000 earthquakes. A bookshelf faulting model for the SISZ has been already proposed (Einarsson et al., 1981; Einarsson and Eiriksson, 1982; Einarsson, 1991; Sigmundsson et al., 1995), in order to explain the presence of the pattern of N–S right-lateral faults in an E–W left-lateral transform zone. Because of the apparent absence of large block rotations in the SISZ, this model was not adopted by other authors (Gudmundsson, 1995; Bergerat et al., 1999). On the other hand, the occurrence of blocks slightly rotating cannot be excluded. Also, the rapid succession of eruptions produced lava flows masking most

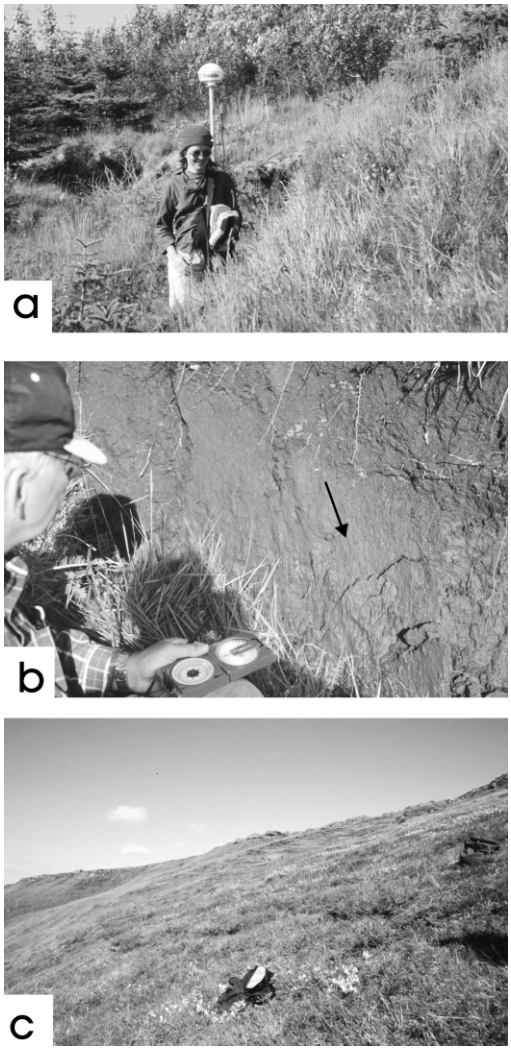

Fig. 11. Photographs of the surface traces of the June 21st 2000 earthquake at Eyvik (first two pictures, see also Fig. 9) and Torfagil (last picture, see also Fig. 10). (a) Normal fault scarp at Eyvik; (b) striated fault surface in the soil layer along the same scarp, with small arrow indicating normal slip (see the fault slip data in the stereoplot of Fig. 10); (c) view towards the north of the open-normal fractures at Torfagil, southwestern flank of Hestfjall mountain (location in Fig. 3), with irregular en-échelon pattern.

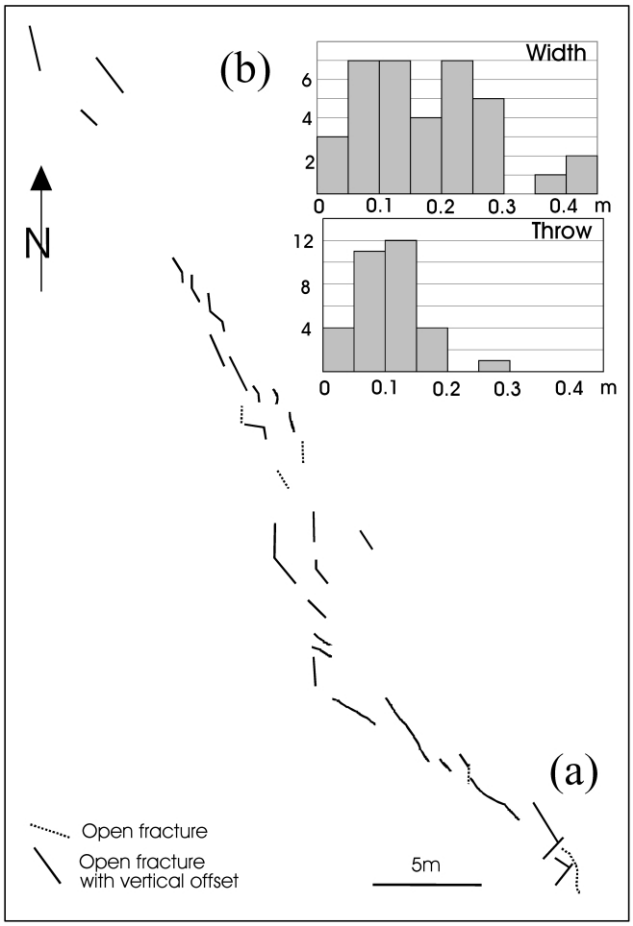

Fig. 12. Surface fissures of the June 21st 2000 earthquake at Torfagil, southwestern flank of the Hestfjall mountain (location in Fig. 3). Mapping done using kinematic GPS (see text). (a) Map of fractures (see also the last picture in Fig. 11); (b) histograms showing the distribution of fracture widths and vertical throws (respectively) versus the number of measurements.

pre-existing outcrops so that few areas give access to the early structural patterns of the SISZ.

The deformation model proposed below aims at reconciling the simple velocity boundary conditions imposed by plate kinematics along the left-lateral, E–W-trending transform zone, and the brittle deformation inside the SISZ, mainly characterised by right-lateral slip along series of N–S-trending faults. The basic assumptions underlying this model are the finite width of the SISZ, its simple shear behaviour and the constant length of the active rift–rift transform fault zone. The main seismic faults are considered as boundaries between blocks in contact side-by-side that can rotate according to the left-lateral motion of the SISZ.

In map view, the rigid blocks are considered as parallelograms (Fig. 13). The northern and southern sides of each parallelogram are the boundaries of the E–W-trending SISZ zone affected by simple shear, while the other two sides are the dextral faults. The faults, which are not assumed to be exactly N–S, have an azimuth θ and a length F (Fig. 13a). The simple shear boundary condition induces block rotation, anticlockwise for an E–W left-lateral shear; the angle of rotation is φ (counted positive anticlockwise; Fig. 13b). The assumed invariability of the SISZ length means that the E–W dimension of each block, L_0, remains constant during the simple shear process so that the initial width between the faults, W_0, varies and becomes W. As a consequence, the rotation induces compression or extension across the fault limits of the block. Under the assumption already mentioned that L_0 is constant for each block, W_0 (Fig 13a), and W (Fig 13b) are given by:

$$W_0 = L_0 \cos\theta \tag{2}$$

$$W = L_0 \cos(\theta - \varphi) \tag{3}$$

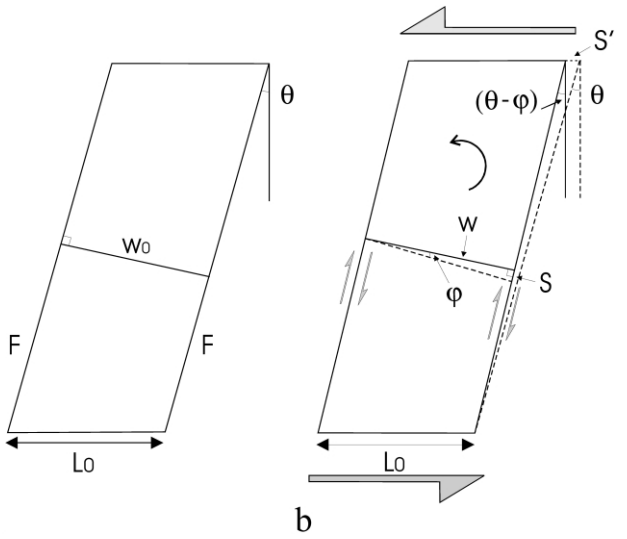

Fig. 13. Geometrical parameters of a simple shear model applied to the SISZ, with situations before (a) and after (b) the co-seismic displacement. In (a), length and azimuth of the approximately N–S-trending faults as F and θ, respectively, block width as W_0, E–W distance between faults as L_0. In (b), co-seismic rotation angle as φ, amount of right-lateral displacement along approximately N–S-trending faults as S, block width as W. The couple of large grey arrows indicates the left-lateral shear in the E–W direction along the SISZ. The couples of small arrows indicate the right-lateral displacement along the approximately N–S-trending faults. The curved arrow shows the inferred sense of block rotation. Amount of left-lateral displacement along the E–W-trending SISZ as S'. The left-lateral simple shear between the two stages is shown in (b) by dashed lines referring to situation (a). Angles and lengths not at scale. See text for discussion.

The variation in block width, ΔW, is:

$$\Delta W = W - W_0 \tag{4}$$

The sign of this difference indicates whether the expected deformation is extensional ($\Delta W > 0$) or compressional ($\Delta W < 0$). In the case of the June 17th and 21st earthquakes, the boundary conditions are as follows:

- the distance, W, between the Árnes and Hestfjall Faults is 17 km according to the map of the *Orkustofnun* (Fig. 3);
- the right-lateral slip along the earthquake faults, S in Fig. 13b, is 0.9 and 1.1 m for the June 17th and 21st earthquakes, respectively (Stefansson et al., 2000), that is, 1 m on average;
- the length, F, of the Árnes and Hestfjall Faults is 16 and 18 km (respectively) as indicated by the distribution of aftershocks, and 25 km in both cases considering the extent of surface traces, giving a reasonable average value of 20 km;
- the value of θ is zero or 10° depending on one considers the Árnes Fault or the Hestfjall Fault as the most typical type of block-bounding fault.

According to the rigid block rotation hypothesis, the angle of rotation, φ, is related to the amount of right-lateral slip, S (Fig. 13b). It is given by:

$$\tan \varphi = S/W \tag{5}$$

For the values listed above, $W = 17$ km and $S = 1$ m, one obtains $\tan \varphi = 5.9 \times 10^{-5}$, that is an angle of rotation of 12″. Because the block rotation results from simple shear along the SISZ, the rotation angle depends on the amount of left-lateral slip, S', along the E–W direction as follows ($F\cos\theta$ being the N–S width of the SISZ, see Fig. 13):

$$\tan \varphi = S'/(F\cos\theta) \tag{6}$$

Thus, the calculated left-lateral slip in the E–W direction, S', is approximately 1.2 m for an average fault length, F, of 20 km. That S and S' have comparable values is not surprising, because in this case the width and the length of the faulted block do not differ markedly.

Coming back to Eqs. (2) and (3), the fault-perpendicular change in block width, ΔW, can be evaluated. In the case of the June 17th earthquake, with $W = 17$ km, $\theta = 0°$ and $\varphi = 12''$, one obtains $\Delta W = -0.03$ mm. Because this variation of width is negligible, the expected behaviour of the Árnes Fault can be regarded neutral in terms of fault-perpendicular compression and extension, implying pure right-lateral strike-slip.

In the case of the June 21st earthquake, according to the same equations, with $W = 17$ km, $\theta = 10°$ and $\varphi = 12''$, the same equations yield a positive value, $\Delta W = 0.18$ m. An increase in block width is thus expected, implying fault-perpendicular extension. As a consequence, the expected behaviour of the Hestfjall Fault includes not only right-lateral strike-slip, but also some extension. This theoretical result is interesting because it is in good agreement with the suspicion of normal faulting and fissure opening observed along the Hestfjall Fault.

5.4. Instantaneous rotation versus finite rotation in the South Iceland Seismic Zone

With respect to the whole deformation of the SISZ, the co-seismic features are in good agreement with a simple shear model involving anticlockwise block rotation. This model accounts for the relationships between the left-lateral movement along the E–W-trending SISZ and the right-lateral displacement of the N–S-trending faults like the Árnes and Hestfjall faults as well as faults from major historical earthquakes. In this paper we simply consider the last increments of the SISZ seismic deformation and we do not aim at analysing the geological evolution of the SISZ during the whole Quaternary period.

It is worth noting, however, that some geometrical and mechanical similarities have been pointed out between the present-day fault patterns issued from seismological analyses and the Pleistocene fault patterns revealed by structural geology studies (e.g. Gudmundsson, 1995; Bergerat et al., 1998). These local studies suggested that the finite rotation, if any, is small. In contrast, a raw linear extrapolation of our

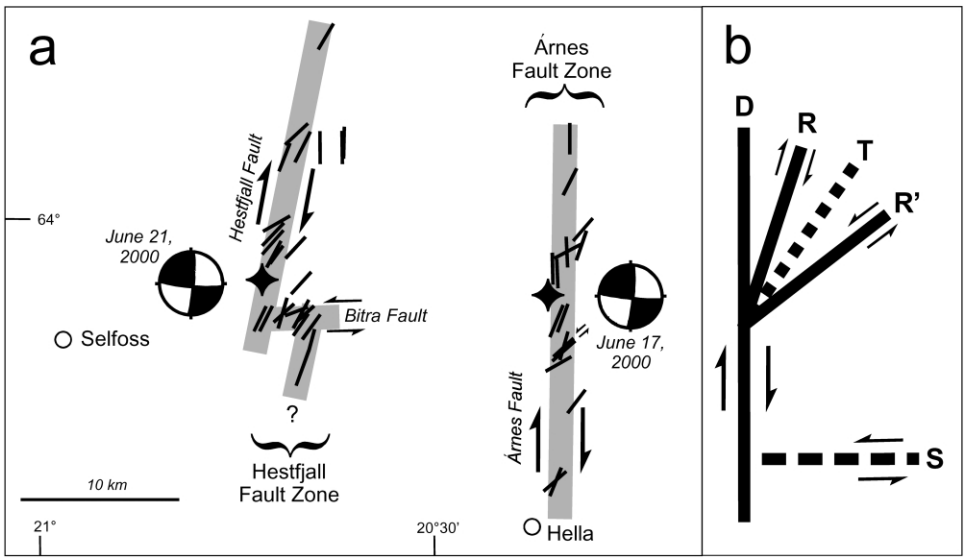

Fig. 14. Summary and tectonic interpretation of the fault pattern of the June 17th and 21st 2000 earthquakes in the SISZ. (a) Interpretative map of the main faults (shown as thick grey lines), with the distribution of the surface fissures (black lines) of the earthquakes adapted from the map of *Orkustofnun*. Epicentres of the two major earthquakes as stars, with the focal mechanisms added as beachballs (compressional quadrants left white). Sense of strike-slip motion indicated by couples of arrows (right-lateral for the Árnes Fault and Hestfjall Fault, left-lateral for the Bitra Fault). (b) Tectonic scheme of the Riedel's type distribution of active faults related to the June 2000 earthquakes. Main N–S-trending right-lateral fault zone, SISZ-perpendicular, as D. NNE–SSW-trending Riedel's right-lateral fault as R. ENE–WSW-trending Riedel's left-lateral fault as R′. NE–SW-trending tensile fracture as T (dotted). The Bitra-type Fault, left-lateral and SISZ-parallel, is added as S (dashed).

results through time would yield large amounts of rotation. Therefore two questions cropped up: is this model applicable to the SISZ since the beginning of its activity? In this case, what would be the implications in terms of deformation?

Based on simple consideration of plate kinematics, the velocity of the long-term left-lateral displacement along the SISZ certainly falls in the range 1–2 cm/yr; the large uncertainty is mainly related to the amount of extension accommodated in the West Volcanic Zone, which is a matter of debate because the GPS-based determination of displacement (Sigmundsson et al., 1995) does not reflect the long-term velocity (Gudmundsson, 2000). Adopting these bounds, the sinistral E–W displacement $S' = 1.2$ m estimated earlier based on consideration of the dextral N–S displacement $S = 1.0$ m would require strain accumulation during a time span of 120–240 years. This is a reasonable value with respect to the average duration of about 140 years of the seismic cycle in the SISZ estimated by Stefansson and Halldorsson (1988), which brings indirect confirmation of our estimate of the left-lateral displacement, S'.

Considering that the SISZ has been active since about 1 Ma as a major transform zone (K. Saemundsson, pers. comm.), extrapolating an angular velocity estimates of 12″ in 120–240 years would result in unacceptably large amounts of finite rotation. The conjugate strike-slip faulting observed along the Árnes and Hestfjall Faults is similar to the older structural pattern observed in the Upper Pleistocene and Holocene rocks of the SISZ. This pattern includes two main structural trends: N0°–N30°E with predominant right-lateral strike-slip faults and N50°–N80°E, with predominant left-lateral strike-slip faults (Bergerat et al., 1999; Bergerat and Angelier, 2000; Gudmundsson, 1995; Passerini et al., 1990; Saemundsson, 1978). This similarity between the fault patterns of the Present and the late Quaternary thus suggest that little rotation has occurred in the areas studied by these authors. Had reorganisations of the fault systems occurred as a consequence of ongoing anticlockwise rotation as mentioned above, a higher complexity of the brittle pattern would be expected in the oldest rock formations of the SISZ than in the recent ones. Note that the importance of the left-lateral ENE–WSW trends has been somewhat underestimated in the literature. The general mapping of recent faults related to major earthquakes (e.g. Einarsson et al., 1981) favoured the N–S dextral faults because their traces are the longest. Detailed mapping, however, demonstrated the occurrence of sinistral ENE–WSW faults (e.g. Bjarnasson et al., 1993). In the kinematic scheme of Fig. 13 the presence of noticeable left-lateral faults (like the Bitra Fault) was ignored; as a result, the calculated amount of anticlockwise rotation is certainly over-estimated. The weakness of a simple bookshelf model of the SISZ may be a direct consequence of not paying proper attention to the ENE–WSW left-lateral faults.

6. Conclusion

Our mapping of surface traces of the June 2000 earthquakes at four main localities demonstrate that the actual active fault pattern is not restricted to the N–S-trending right-lateral strike-slip revealed by the focal mechanisms and the N–S alignment of aftershocks. Within both the Árnes and Hestfjall fault zones, this fault pattern

includes NNE–SSW-trending right-lateral and ENE–WSW-trending left-lateral strike-slip faults, as well as extensional features such as open fractures. In addition, dip-slip normal faults were observed at Eyvik, along the Hestfjall Fault. Because we could define the mechanisms of fault segments of different orientations, the comparison between our data and the general preliminary map presented by the *Orkustofnun* (Fig. 3) provides some insights regarding the distribution of fault movements during the June 2000 earthquakes. For instance, in light of the results obtained at Bitra, the NE–SW-trending rupture traces forming an E–W en-échelon pattern near the southern tip of the Hestfjall Fault should be interpreted as a distinctive left-lateral fault segment, named the Bitra Fault (Fig. 14a). As a consequence, these southern rupture traces should not be used to define the general orientation of the right-lateral Hestfjall Fault. This comment can explain why the N10°E trend of the Hestfjall Fault, mentioned in our model, differs from the N2°W trend suggested by the overall distribution of microearthquakes within the Hestfjall fault zone (which includes the Bitra Fault, as Fig. 14a shows). Our mapping at Mykjunes also confirms that in more detail the presence of Riedel's type conjugate fault segments, left- and right-lateral, introduces complexity in the pattern of large, approximately N–S-trending, right-lateral fault lines. Although we could not examine all outcrops, this observation may also account for the presence in the *Orkustofnun* map of numerous rupture traces that trend NNE–SSW to ENE–WSW, oblique to the large fault lines. As Fig. 13b suggests, the azimuthal distribution of the earthquake fractures can be accounted for by the presence of open fissures as well as right-lateral and left-lateral strike-slip faults forming conjugate patterns. The NE–SW trend of the compression axis indicated by these conjugate systems is oblique to, and mechanically compatible with, both the approximately N–S strike of the main dextral Árnes and Hestfjall faults and the nearly E–W strike of the Bitra Fault segment (Fig. 14).

Considering the complexity of the surface traces of the June 17th and 21st 2000 earthquakes and of historical earthquakes as well (e.g. Einarsson and Eiriksson, 1982; Bjarnasson et al., 1993; Bergerat et al., 2003), one should note that numerous secondary fractures and faults developed during these earthquakes. Because they affect the Earth's surface, the secondary fractures and faults have a direct impact on society (Belardinelli et al., 2000). In the past as well as during the June 2000 earthquakes, these earthquake fractures and faults caused the collapse of many farm buildings and a variety of damages in the SISZ (Thoroddsen, 1899; Stefansson et al., 2000), which is a dire concern in earthquake hazard evaluation and civil engineering. Analysing these surface faults is therefore important in terms of seismic hazard prevention.

Acknowledgements

This work was supported by a grant of the European Commission (SMSITES project, contract EVR1-CT-1999-40002) and by a grant of the French Polar Institute (IFRTP, Arctic Program, project no. 316). We would like to thank A. Gudmundsson for his help in locating and choice of the surface traces, C. Homberg for her participation in mapping the Torfagil and Eyvik fault segments, and R. Stefansson for discussions about the June 17th and 21st 2000 earthquakes. Reviews by K. Saemundsson and K. Scharer, and editorial suggestions of J.P. Evans improved the clarity of the final manuscript and are gratefully acknowledged.

References

Angelier, J., Bergerat, F., Dauteuil, O., Villemin, T., 1997. Effective tension-shear relationships in extensional fissure swarms, axial rift of northeastern Iceland: morphological evidences. Journal of Structural Geology 19 (5), 673–685.

Belardinelli, M.E., Bonafede, M., Gudmundsson, A., 2000. Secondary earthquake fractures generated by a strike-slip fault in the South Iceland Seismic Zone. Journal of Geophysical Research 105, 13613–13629.

Bergerat, F., Angelier, J., 2000. The South Iceland Seismic Zone: tectonic and seismotectonic analyses revealing the evolution from rifting to transform motion. Journal of Geodynamics 29, 211–231.

Bergerat, F., Angelier, J., 2001. Mécanismes des failles des séismes des 17 et 21 Juin 2000 dans la Zone Sismique Sud-Islandaise d'après les traces de surface des failles d'Árnes et de l'Hestfjall. Comptes Rendus Académie des Sciences 333, 35–44.

Bergerat, F., Gudmundsson, A., Angelier, J., Rögnvaldsson, S.Th., 1998. Seismotectonics of the central part of the South Iceland Seismic Zone. Tectonophysics 298, 319–335.

Bergerat, F., Angelier, J., Verrier, S., 1999. Tectonic stress regimes, rift extension and transform motion: the South Iceland Seismic Zone. Geodinamica Acta 12, 303–319.

Bergerat, F., Angelier, J., Gudmundsson, A., Torfason, H., 2003. Push-ups, fracture patterns, and palaeoseismology of the Leirubakki Fault, South Iceland. Journal of Structural Geology 25(4), 591–609.

Bjarnasson, I.Th., Cowie, P., Anders, M.H., Seeber, L., Scholz, C.H., 1993. The 1912 Iceland earthquake rupture: growth and development of a nascent transform system. Bulletin of the Seismological Society of America 83, 416–435.

Bödvarsson, R., Rögnvaldsson, S.Th., Jakobsdottir, S.S., Slunga, R., Stefansson, R., 1996. The SIL data acquisition and monitoring system. Seismological Research Letters 67, 35–46.

DeMets, C., Gordon, R.G., Argus, F., Stein, S., 1990. Current plate motions. Geophysical Journal International 101, 425–478.

DeMets, C., Gordon, R.G., Argus, F., Stein, S., 1994. Effect of recent revisions to the geomagnetic reversal time scale on estimates of current plate motions. Geophysical Research Letters 21, 2191–2194.

Einarsson, P., 1991. Earthquake and present-day tectonism in Iceland. Tectonophysics 189, 261–279.

Einarsson, P., Eiriksson, J., 1982. Earthquake fractures in the districts Land and Rangárvellir in the south Iceland seismic zone. Jökull 32, 113–120.

Einarsson, P., Björnsson, S., Foulger, G., Stefansson, R., Skaftadottir, Th., 1981. Seismicity pattern in the South Iceland Seismic Zone. In: Simpson, D.W., Richards, P.G. (Eds.), Earthquake Prediction: An International Review, AGU Maurice Ewing Series 4, Washington DC, pp. 141–151.

Gudmundsson, A., 1995. Ocean-ridge discontinuities in Iceland. Journal of the Geological Society 152, 1011–1015.

Gudmundsson, A., 2000. Dynamics of volcanic systems in Iceland: example of tectonism and volcanism at juxtaposed hot spot and mid-ocean ridge systems. Annual Review of Earth and Planetary Sciences 28, 107–140.

Helgason, J., 1985. Shifts of the plate boundary in Iceland: some aspects of Tertiary volcanism. Journal of Geophysical Research 90, 10084–10092.

Johannesson, H., Jakobsson, S.P., Saemundsson, K., 1990. Geological map of Iceland, sheet 6, south Iceland. Icelandic Museum of Natural History and Iceland Geodetic Survey, Reykjavik, scale 1:250,000.

Karnik, V., 1969. Seismicity of the European Area, Part I, Reidel, Dordrecht, Holland.

Passerini, P., Sguazzoni, G., Marcucci, M., Zan, L., 1990. Slickensides in Western and Southern Iceland: data from Langavatn, Burfell and Vördufell. Ofioliti 15, 191–196.

Saemundsson, K., 1974. Evolution of the axial rift zone in northern Iceland and the Tjörnes Fracture Zone. Geological Society of America Bulletin 85, 495–504.

Saemundsson, K., 1978. Fissure swarms and central volcanoes of the neovolcanic zones in Iceland. Geological Journal Special Issue 10, 415–432.

Sigmundsson, F., Einarsson, P., Bilham, R., Sturkell, E., 1995. Rift-transform kinematics in south Iceland: deformation from Global Positioning System measurements, 1986 to 1992. Journal of Geophysical Research 100, 6235–6248.

Stefansson, R., Halldorsson, P., 1988. Strain release and strain build-up in the South Iceland Seismic Zone. Tectonophysics 152, 267–276.

Stefansson, R., Bödvarsson, R., Slunga, R., Einarsson, P., Jakobsdottir, S.S., Bungum, H., Gregersen, S., Havskov, J., Hjelme, J., Korhonen, H., 1993. Earthquake prediction research in the South Iceland Seismic Zone and the SIL project. Bulletin of the Seismological Society of America 83, 696–716.

Stefansson, R., Gudmundsson, G.B., Halldórsson, P., 2000. The two large earthquakes in the South Iceland Seismic Zone on June 17 and 21, 2000. URL: http://www.vedur.is.

Thoroddsen, T., 1899. Jardskjalftar a Sudurlandi (Earthquakes in South Iceland), Hid Íslensjska Bokmenntafelag, Copenhagen.

Ward, P.L., 1971. New interpretation of the geology of Iceland. Geological Society of America Bulletin 82, 2991–3012.